Identification of Nidogen 1 as a lung metastasis protein through secretome analysis

Maša Alečković,[1] Yong Wei,[1] Gary LeRoy,[1] Simone Sidoli,[2] Daniel D. Liu,[1] Benjamin A. Garcia,[2] and Yibin Kang[1]

[1]Department of Molecular Biology, Princeton University, Princeton, New Jersey 08544, USA; [2]Epigenetics Program, Department of Biochemistry and Biophysics, Perelman School of Medicine, University of Pennsylvania, Philadelphia, Pennsylvania 19104, USA

Secreted proteins play crucial roles in mediating tumor–stroma interactions during metastasis of cancer to different target organs. To comprehensively profile secreted proteins involved in lung metastasis, we applied quantitative mass spectrometry-based proteomics and identified 392 breast cancer-derived and 302 melanoma-derived proteins secreted from highly lung metastatic cells. The cancer-specific lung metastasis secretome signatures (LMSSs) displayed significant prognostic value in multiple cancer clinical data sets. Moreover, we observed a significant overlap of enriched pathways between the LMSSs of breast cancer and melanoma despite an overall small overlap of specific proteins, suggesting that common biological processes are executed by different proteins to enable the two cancer types to metastasize to the lung. Among the novel candidate lung metastasis proteins, Nidogen 1 (NID1) was confirmed to promote lung metastasis of breast cancer and melanoma, and its expression is correlated with poor clinical outcomes. In vitro functional analysis further revealed multiple prometastatic functions of NID1, including enhancing cancer cell migration and invasion, promoting adhesion to the endothelium and disrupting its integrity, and improving vascular tube formation capacity. As a secreted prometastatic protein, NID1 may be developed as a new biomarker for disease progression and therapeutic target in breast cancer and melanoma.

Tumor-secreted factors play crucial roles in orchestrating the dynamic evolution of the microenvironment at primary and distant sites (Peinado et al. 2011; Quail and Joyce 2013; Alečković and Kang 2015). Understanding how they facilitate tumor–stroma interactions has not only created an increasingly detailed molecular model of cancer metastasis but also led to the development of novel markers and therapeutics. For example, during osteolytic bone metastasis, tumor-secreted proteins activate osteoclast differentiation, leading to bone matrix degradation and the release of growth factors that promote metastatic outgrowth, completing a "vicious cycle" (Weilbaecher et al. 2011; Ell and Kang 2012; Ren et al. 2015). While the pulmonary metastatic microenvironment is not as well characterized as that in bone metastasis, accumulating evidence points to secreted proteins as instructive players during lung metastasis. Communication between primary and secondary sites via tumor-secreted factors, such as lysyl oxidase (a hypoxia-induced extracellular matrix [ECM] remodeling enzyme) or the exosomal MET receptor, facilitates the formation of a premetastatic lung parenchyma that favors metastatic colonization (Kaplan et al. 2005; Erler et al. 2006; Peinado et al. 2012). Likewise, miR-200 promotes lung metastatic colonization by altering the breast cancer secretome via direct inhibition of Sec23a-mediated secretion of metastasis-suppressive proteins, including Igfbp4 and Tinagl1 (Korpal et al. 2011), further supporting the hypothesis that cancer secretomes play instructive roles during lung metastasis.

While secreted proteins have long been appreciated as markers and mediators of metastasis, high-throughput and comprehensive analysis of the secretome only became possible via recent advances in mass spectrometry (MS). MS analysis of the ECM revealed different ECM protein signatures associated with organ-tropic metastasis of different cancer types (Reticker-Flynn et al. 2012; Naba

et al. 2014a,b). Our recent application of MS analysis of bone metastasis secretomes has led to the identification of novel bone metastasis proteins that may serve as biomarkers or therapeutic targets (Blanco et al. 2012). Application of the global proteomic analysis approach to lung metastasis secretomes has the potential to reveal the relatively little-known tumor–stroma interactions in lung metastasis.

In this study, we used quantitative proteomic analysis to profile the secretomes of lung metastatic breast cancer and melanoma cells of varying metastatic ability and obtain cancer-specific lung metastasis secretome signatures (LMSSs). These signatures correlated with poor prognosis and metastatic relapse in clinical data sets and contained strikingly similar types of proteins engaged in common biological processes despite little overall protein overlap. The secretomes and LMSSs comprise known and novel cancer- and metastasis-related proteins and may serve as databases to guide future functional studies in the metastasis field. Following the identification of highly overrepresented proteins in secretomes of aggressively lung metastatic cells, we examined Nidogen 1 (NID1) as a candidate promoter of lung metastasis in both cancer types. Xenograft experiments using overexpression and knockdown models validated its role in promoting lung metastasis. This phenotype was particularly strong at early stages of metastatic colonization, consistent with our in vitro findings that NID1 improved cancer cell migration and invasion, adhesion to endothelial cells (ECs), vascular permeability, and tube formation. Moreover, *NID1* expression correlated with poor prognosis and lung relapse in breast cancer and melanoma patient data sets. These results indicate NID1 as a potential biomarker for high risk of lung metastasis as well as a therapeutic target for preventing or reducing lung metastasis.

Results

In vivo selection of lung metastatic derivatives of the HTB140 human melanoma cell line

To quantitatively profile the lung metastasis-associated cancer secretome, we used isogenic cell lines that have a similar origin and genetic background but drastically different potential to metastasize to the lungs. Such isogenic sublines have been typically derived by in vivo selection from lung metastatic lesions generated by the parental cell line (Pollack and Fidler 1982). Minn et al. (2005) previously used such a strategy to establish the lung-tropic sublines LM2-A and LM2-B from the MDA-MB-231 human breast cancer cell line. In order to identify secreted lung metastatic genes that have functional involvement in diverse cancer types, we also derived lung metastatic sublines from the human melanoma cell line HTB140, which was established previously from lymph node metastases of a male cutaneous melanoma patient (Fogh et al. 1977). We isolated several HTB140 sublines from individual metastatic lung nodules after tail vein inoculation of the parental cell line into mice. Testing of the lung metastatic potential of these variants confirmed that the in

vivo selected sublines colonized the lung more efficiently than the parental HTB140 cells, displaying an increase of 20-fold (LM1a) to 100-fold (LM1-744) in lung metastatic burden (Supplemental Fig. S1A,B). As we selected LM1a and LM1-744 for subsequent proteomic analysis, we assessed their proliferation rates in vitro. Both lung metastatic sublines proliferated at a rate similar to that of the parental HTB140 cell line (Supplemental Fig. S1C), suggesting that the increased lung metastatic ability is not due to a difference in the growth rate of the derivatives. These results established the HTB140 and its sublines as a new isogenic series for studying lung metastasis of melanoma.

Global analysis of breast cancer and melanoma lung metastasis secretomes

Using a SILAC (stable isotope labeling with amino acids in cell culture)-based MS approach (Blanco et al. 2012), proteins released by lung metastatic breast cancer and melanoma sublines were quantified with respect to those secreted by parental cells following cell culture in "heavy" and "light" media, containing heavy or normal arginine and lysine, respectively (Fig. 1A). We performed database searches of the obtained tandem MS (MS/MS) spectra against the human UniProt database and discovered a total of 2320 unique proteins encoded by 2264 genes (Fig. 1B; Supplemental Table S1), proving the high sensitivity of the analysis. Interestingly, while 2116 unique proteins were found in the breast cancer secretome and 1803 were found in the melanoma secretome, >70% of all identified proteins (1599) were discovered in both (Fig. 1B). In line with this, gene ontology (GO) enrichment analyses demonstrated enrichment of similar biological process and molecular function annotations in both cancer secretomes (Fig. 1C,D; Supplemental Fig. S2A–D), the majority of which related to extracellular processes, including extracellular structure organization, cellular component movement, and transport. The melanoma secretome was additionally enriched in proteins engaged in vascular development.

We asked whether filtering methods eliminating possible intracellular contaminants that may have been liberated nonspecifically as a consequence of cell death, as used in previous secretome analyses (Korpal et al. 2011; Blanco et al. 2012; Jin et al. 2012), would be required or whether our secretome lists consisted mostly of extracellular proteins and could be used unprocessed. Indeed, 55% of proteins were mapped to the "extracellular region" in GO, including compartments such as "extracellular exosome," "cell surface," and "external side of the plasma membrane." Surveying exosome databases Exo-Carta (Mathivanan and Simpson 2009) and Vesiclepedia (Kalra et al. 2012) for human proteins verified previously at the protein level further revealed that the majority of secreted proteins (80%–90%) was exosomal. Most importantly, >90% of secretome proteins associated with at least one extracellular compartment annotation interrogated (Fig. 1E; Supplemental Table S1), validating our method of secretome-focused proteomics and permitting
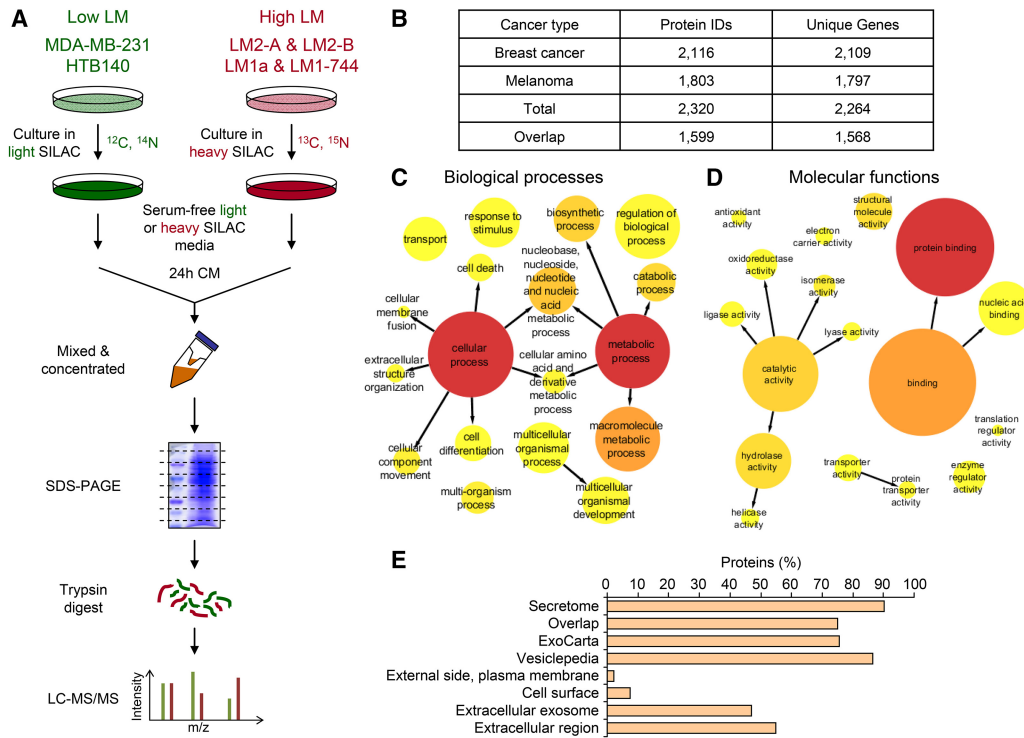
Figure 1. The SILAC-based MS approach comprehensively profiles breast cancer and melanoma secretomes. (*A*) Schematic overview of the MS-based quantitative proteomics analysis using SILAC. Breast cancer and melanoma parental cell lines were cultured in light SILAC medium, whereas their respective lung metastatic sublines were cultured in heavy SILAC medium. Serum-free light medium and heavy conditioned medium (CM) were then mixed, processed, and analyzed by MS. (*B*) The number of protein IDs and unique genes identified by our secretome analysis. (*C,D*) Visualization of GO analysis of overrepresented biological process (*C*) and molecular function (*D*) GO Slim terms of the breast cancer secretome. A very similar enrichment was found in the melanoma secretome (see Supplemental Fig. S2A,B). (*E*) Subcellular compartment analysis of all identified proteins. GO compartments were "extracellular region" (GO: 0005576), "extracellular exosome" (GO: 0070062), "cell surface" (GO: 0009986), and "external side of plasma membrane" (GO: 0009897). Secretome denotes proteins found in at least one of the analyzed extracellular compartments. Overlap includes proteins found in both exosome databases.

the use of the unfiltered lists for subsequent analyses. Furthermore, these results suggest that intracellular proteins released nonselectively due to, for instance, serum starvation-induced apoptosis may constitute a minor part of the overall proteins identified in our secretome analysis and do not need to be excluded in downstream analyses.

Next, we examined the concordance between gene and protein expression profiles of secreted proteins in order to guide any subsequent data analysis that integrates our proteomic results into transcriptomic data sets. While overall correlation between mRNA and protein levels is usually expected, extracellular proteins may experience a substantial degree of regulation at the post-transcriptional level (Vogel and Marcotte 2012), including translation, processing, and secretion. In fact, we observed significant positive correlation, with coefficients between 0.4 and 0.5 (Supplemental Fig. S3A–D), which correspond well to those reported in other mRNA–protein correlation studies of intracellular proteins (Vogel and Marcotte 2012). This result suggests that secretion may not constitute a further deviation of the protein level from the mRNA expression level. It also provides a rationale for using transcriptomic data of secreted proteins for analyses

for which no protein data are yet available, such as evaluation of their prognostic value. Nevertheless, the overall positive correlation offers a global validation of our protein level results, while the substantial degree of deviation indicates that the proteomic data harbor new information on the protein level that was missed in transcriptomic studies. For instance, fibronectin (FN1), although more abundant in secretomes of lung metastatic sublines compared with parental cells in both breast cancer and melanoma models, showed elevated mRNA expression only in melanoma but not in the breast cancer sublines (Supplemental Fig. S3A–D). Similarly, nephroblastoma overexpressed (NOV) was elevated in secretomes but not transcriptomes of lung-tropic breast cancer cells relative to the parental MDA-MB-231 (Supplemental Fig. S3A,B). Consistent with the elevated levels of FN1 and NOV in the lung metastatic secretomes, both proteins have been associated previously with cell invasion and metastasis (Akiyama et al. 1995; Benini et al. 2005; Perbal 2006; Vallacchi et al. 2008; Liu et al. 2015; Mehta et al. 2015) as well as higher risk of metastasis and poor prognosis in cancer patients (Glukhova et al. 2001; Perbal et al. 2008, 2009; Malik et al. 2010; Zhang et al. 2013; Fernandez-Garcia et al. 2014; Ueda et al. 2015). These initial analyses

validate the technical quality of our secretome analyses and indicate the potential utility of such an approach for identifying cancer-related secreted proteins that may not be identified through transcriptomic analyses.

Generation of cancer-specific LMSSs

Examining proteins whose levels are altered at least twofold in secretomes of metastatic derivatives relative to parental cells, we detected 149 and 165 unique proteins elevated in secretion from lung-tropic LM2-A and LM2-B cells, respectively, compared with MDA-MB-231. We also identified 232 and 194 proteins elevated in secretion from lung metastatic LM1a and LM1-744 cells, respectively, relative to HTB140. Conversely, 307, 220, 120, and 75 proteins were reduced in secretion from LM2-A, LM2-B, LM1a, and LM1-744 cell lines compared with their respective parental cell lines.

We generated cancer-specific LMSSs by considering proteins to be up-regulated (Up-LMSS) if secretion from both lung metastatic sublines was higher by twofold or more relative to the parental cell line. Any proteins that were increased in secretion by twofold or more in only one of the two sublines were also included in the signature as long as they were not present at decreased levels in the other subline. Similarly, the Down-LMSS was generated using proteins whose secretion from at least one of the two lung metastatic sublines was lower by twofold or more compared with the parental cell line, as long as it did not have the opposite trend in the other subline. This analysis yielded signatures of 149 and 210 up-regulated (Up-LMSS) and 243 and 92 down-regulated (Down-LMSS) proteins in breast cancer and melanoma, respectively (Fig. 2A,B; Supplemental Tables S2–S5). The signatures had 20 up-regulated and 16 down-regulated proteins in common (Fig. 2C). Considering that the global secretomes displayed over 70% overlap, the number of common proteins in Up-LMSS and Down-LMSS (10%–20%) appeared smaller than expected.

We explored the GO enrichment in the cancer-specific Up-LMSS data sets and found that, despite little protein overlap, many overrepresented pathways and protein categories were identical (Supplemental Tables S6–S9). More specifically, 16 of 27 (59%) significantly overrepresented biological processes and seven of nine (78%) molecular functions in breast cancer were also found in melanoma. Furthermore, all common biological processes were GO annotations pertinent to tumorigenesis and metastasis, such as "cell adhesion," "response to wounding," and "cell movement" (Fig. 2D). Similarly, among the most significantly overrepresented molecular function annotations were cancer/metastasis-related functions, including "growth factor binding" and "receptor binding" (Fig. 2D).

Finally, to understand how these diverse sets of proteins are interconnected, we analyzed the interaction networks of cancer-specific LMSSs and observed well-linked networks that clustered into densely connected nodes based on protein families or biological processes (Fig. 2E,F). Both LMSS networks contained similar clusters, such as ECM components, ECM-modifying enzymes, defense re-

sponse proteins, and protein metabolism (transcription elongation factors and ribosome and proteasome subunits). Most importantly, despite an overall different pool of proteins among the signatures, the similarity in clustering patterns between the two interactomes further underscored the global similarity between breast cancer and melanoma LMSSs.

Association of LMSS proteins with experimental and clinical lung metastasis

To examine whether findings from our experimental cell line-profiling system are relevant to metastasis, we first manually inspected the 626 LMSS proteins for clinical and experimental association with cancer or metastasis (UniProt knockdown gene summary, The Cancer Gene Census [Futreal et al. 2004], and PubMed search). At least 307 proteins, including TNC, SERPINE2, and CTSB, emerged as known promoters of lung metastatic progression (Benini et al. 2005; Vasiljeva et al. 2006; Oskarsson et al. 2011; Sevenich et al. 2011; Wagenblast et al. 2015). Furthermore, the breast cancer Up-LMSSs contained MMP1, MMP2, and SPARC, which are well-known metastasis mediators in breast cancer (Minn et al. 2005; Vallacchi et al. 2008; Liu et al. 2015). On the other hand, known metastasis promoters found in the melanoma Up-LMSSs included MIA (Bosserhoff and Buettner 2002), GPNMB (Maric et al. 2013), and ADAM10 (Lee et al. 2010).

To further investigate the clinical relevance of the LMSSs, we evaluated the prognostic significance of LMSSs in clinical data sets of breast cancer. Using the composite Kaplan-Meier (KM) Plotter data set (Gyorffy et al. 2010), we found that breast cancer patients with tumors overexpressing the top 40 Up-LMSS genes had shorter distant metastasis-free survival (DMFS) than those expressing low levels (Fig. 3A–C), particularly among ER-negative patients (Fig. 3B) Conversely, breast cancer patients with high levels of the top 40 Down-LMSS genes showed significantly prolonged DMFS compared with patients with low expression (Fig. 3D). Likewise, this trend was more apparent among the ER-negative patient population (Fig. 3E) and, to a lesser extent, in ER-positive patients (Fig. 3F). Similarly, using The Cancer Genome Atlas (TCGA) skin cutaneous melanoma data set, patients with high levels of the top 40 Down-LMSS genes displayed significantly prolonged overall survival relative to those expressing high levels (Fig. 3G), although a similar analysis using the Up-LMSS did not show a statistically significant result.

Using gene set enrichment analysis (GSEA) (Subramanian et al. 2005), we examined enrichment of lung metastasis signatures in the list of genes from the published clinical data set EMC286 (Wang et al. 2005) ranked by their degree of overexpression in breast cancer patients who suffered metastasis compared with those who remained disease-free. Interestingly, enrichment of Up-LMSS was significant ($P = 0.011$) only in patients with lung metastasis (Fig. 3H) but not the entire metastatic patient cohort ($P = 0.978$) (Fig. 3I), which indicates the specificity of the signature for lung metastasis. Overall, these results indicate that our LMSSs have clinical significance
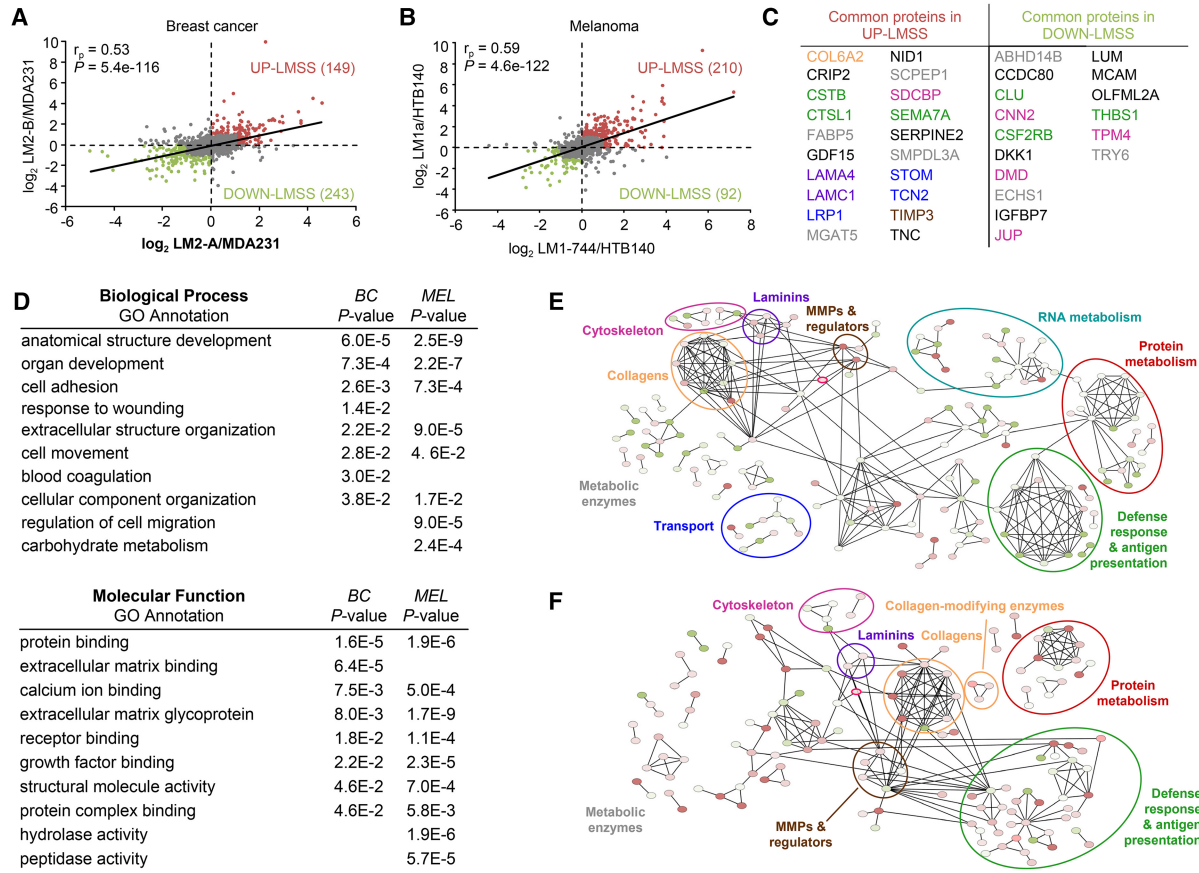
Figure 2. Secretome analysis reveals cancer-specific LMSSs. (*A,B*) Correlation of pairwise secretome comparisons of breast cancer cell lines LM2-A versus MDA-MB-231 and LM2-B versus MDA-MB-231 (*A*) as well as melanoma cell lines LM1a versus HTB140 and LM1-744 versus HTB140 (*B*). Pearson correlation coefficients (r_p) are displayed with corresponding *P*-values. The numbers of proteins found at least twofold higher (red) or lower (green) in lung metastatic sublines compared with parental are highlighted. Proteins found in only one cell line within a comparison were excluded from the correlation analysis but included in the LMSSs. (*C*) List of common proteins in Up-LMSSs and Down-LMSSs of breast cancer and melanoma. Colors correspond to clusters in *E* and *F*. (*D*) Breast cancer and melanoma Up-LMSSs were subjected to GO enrichment analysis. (*E,F*) Interactomes of breast cancer (*E*) and melanoma (*F*) LMSSs. Several protein clusters are highlighted. NID1 is circled in pink. Proteins released at higher (red) or lower (green) levels from lung metastatic sublines compared with parental cell lines are color-coded.

that could be useful prognostic tools for clinical lung metastasis.

NID1 as a candidate lung metastasis promoter in breast cancer and melanoma

While our proteomic analysis identified numerous established metastasis regulators, the signatures likely harbor as yet undiscovered regulators of lung metastasis. We focused our functional study on NID1 based on the following observations. NID1 was among the 20 common Up-LMSS proteins elevated in the secretomes of both breast cancer and melanoma sublines (Fig. 2C); bridged several GO terms enriched in both Up-LMSSs, such as "extracellular structure organization" and "cell adhesion"; and displayed direct and indirect interaction with many cancer secretome proteins, particularly other ECM components (Supplemental Fig. S4A,B). This is in agreement with its known role in facilitating ECM formation (Aumailley

et al. 1993; Dziadek 1995; Tunggal et al. 2003) and cell attachment to a NID1-containing ECM (Dedhar et al. 1992; Dong et al. 1995; Yi et al. 1998). Furthermore, NID1 was shown to enhance cell motility (Pedrola et al. 2015) and is elevated in the blood of cancer patients compared with healthy controls (Zhang et al. 2012; Khan et al. 2014; Li et al. 2015), making it an attractive candidate for experimental assessment in our lung metastasis models.

Before initiating experimental evaluation of the role of NID1 in lung metastasis, we confirmed its up-regulation in conditioned medium (CM) of lung metastatic derivatives relative to parental cell lines (Fig. 4A,B). Specifically, lung-tropic LM2-A (fourfold) and LM2-B (fivefold) cells secreted more NID1 than MDA-MB-231 cells (Fig. 4A). Similarly, LM1a (fivefold) and LM1-744 (sixfold) sublines secreted higher levels of NID1 compared with HTB140 cells (Fig. 4B). However, analysis of mRNA expression levels by real-time quantitative PCR (RT-qPCR) did not align well with the protein levels, as most lung metastatic
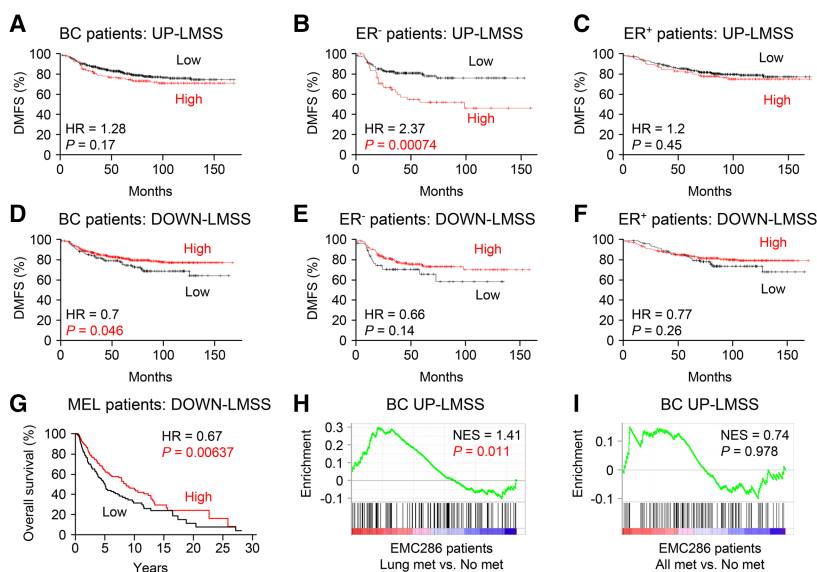
Figure 3. Clinical analysis of LMSSs in patient data sets. (*A–F*) KM plots of DMFS of all (*A,D*), ER-negative (*B,E*), and ER-positive (*C,F*) breast cancer patients, stratified by the upper quartile expression of the top 40 Up-LMSS genes (*A–C*) and the lower quartile expression of the top 40 Down-LMSS genes (*D–F*). KM Plotter, $n = 664$ all; $n = 227$ ER⁻; $n = 437$ ER⁺. (*G*) KM plot of overall survival of melanoma patients stratified by median expression of the top 40 Down-LMSS genes. TCGA melanoma, $n = 470$. (*H,I*) The breast cancer Up-LMSS was used as a gene set and tested for enrichment via gene set enrichment analysis (GSEA) in the list of genes ranked by degree of overexpression in primary breast cancer tumors from patients in the EMC286 patient data set who developed lung metastasis (*H*) or any type of metastasis (*I*) as compared with patients who remained metastasis-free. (NES) Normalized enrichment score; (HR) hazard ratio. Log-rank test *P*-values are displayed.

variants showed expression levels similar to, or even reduced compared with, the respective parental cell lines (Fig. 4A,B). Hence, its regulation at the post-transcriptional level further underscores the value of secretome analysis in identifying novel metastasis proteins.

Overexpression of NID1 promotes lung metastatic progression in vivo

To examine the importance of NID1 in lung metastasis, MDA-MB-231 cells stably overexpressing NID1 (Fig. 4C) were inoculated into mouse via tail veins, leading to a 10-fold increase in lung metastasis (Fig. 4D,E) and shorter overall survival (Fig. 4F) compared with controls. This phenotype did not seem to stem from faster proliferation, since primary tumors derived from overexpression cells grew slower than controls in vivo, as evident from the reduced tumor size (Supplemental Fig. S5A) and weight (Supplemental Fig. S5B). To rule out cell population drifts during the stable transfection and selection of NID1-overexpressing cells from the heterogeneous parental MDA-MB-231 cell line, the single-cell-derived SCP28 subline was used to confirm the prometastatic role of NID1. SCP28 and the parental MDA-MB-231 cells secrete similar basal levels of NID1 (data not shown) and have similar lung metastatic propensities (Minn et al. 2005). NID1-overexpressing SCP28 cells (Supplemental Fig. S5C) gained significantly increased lung metastasis ability compared with the vector control cells (Supplemental Fig. S5D–F). Similarly, overexpression of NID1 in HTB140 melanoma cells (Supplemental Fig. S5G) led to a threefold increase in lung metastasis (Supplemental Fig. S5H). Notably, the increase in lung metastasis ability occurred at early time points of the in vivo lung colonization assays (1–2 wk), indicating an advantage during seeding and early colonization for NID1-overexpressing cells. NID1 overexpression also caused a modest decrease in primary tumor growth compared with controls in the HTB140 melanoma cell line, although this did not reach

significance (Supplemental Fig. S5I). Taken together, the data from the NID1 overexpression experiments indicate that increased NID1 secretion from breast cancer and melanoma cells promotes their metastatic ability particularly at early steps of metastatic outgrowth in the lung parenchyma.

Loss of NID1 expression hampers lung metastatic progression in vivo

Having established that NID1 is sufficient to drive lung metastatic progression, we next generated stable NID1 knockdown cells to examine whether it also is necessary to support lung metastasis. The melanoma model was used for protein depletion experiments due to higher basal expression levels. Two individual shRNAs decreased *NID1* mRNA levels and secretion of NID1 protein from LM1a cells compared with two independent controls—an empty vector and a scrambled shRNA control (Fig. 4G). Reduction in NID1 secretion inhibited in vivo lung metastasis (Fig. 4H) to varying degrees that were consistent with the remaining NID1 levels. Specifically, NID1-KD2 cells, secreting the lowest NID1 amounts, showed a larger reduction (60-fold) than NID1-KD1 cells (sixfold). Consistent with the reduced primary subcutaneous tumor growth in NID1-overexpressing cells, NID1 knockdown in LM1a cells resulted in increased primary tumor growth (Fig. 4J). Similarly, NID1 knockdown in LM1-744 cells (Supplemental Fig. S6A) dramatically diminished lung metastasis (Supplemental Fig. S6B). These results indicate an essential role for NID1 specifically for metastatic colonization in the lungs.

NID1 enhances migration, invasion, adhesion to the endothelium, vascular permeability, and tube formation in vitro

To elucidate the mechanism underlying NID1-mediated lung metastasis, we examined processes associated with
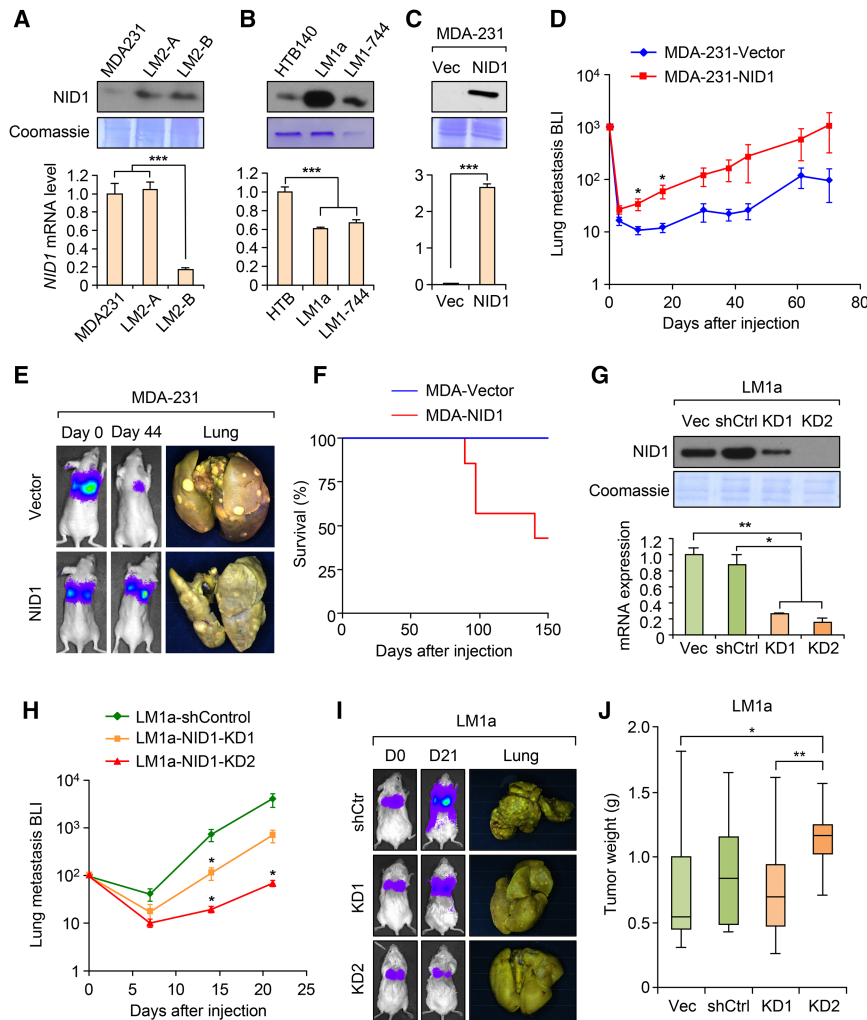
Figure 4. NID1 is increased in CM of lung metastatic derivatives and promotes lung metastasis while reducing tumorigenesis in vivo. (*A–C, top*) Western blot analysis of NID1 in CM of parental and lung metastatic sublines of the MDA-MB-231 human breast cancer cell line (*A*) or the HTB140 melanoma cell line (*B*) and control or NID1-overexpressing MDA-MB-231 cells. (*C, middle*) Coomassie blue staining of the membrane was used as loading control. (*Bottom*) RT-qPCR analysis of *NID1* expression in cells relative to parental cell lines and normalized to *GAPDH* levels. (*D,E*) Bioluminescence imaging (BLI) quantification (*D*) and representative images (*E*) of lung metastasis after tail vein injection of vector- and NID1-overexpressing MDA-MB-231 cells. *n* = 6. (*F*) KM representation of overall survival of mice bearing lung metastases from *D*. *P* = 0.02, *n* = 5; *n* = 7. (*G, top*) Western blot analysis of NID1 levels in CM of control (vector and scrambled shRNA) and NID1 knockdown (KD1 and KD2) LM1a cell lines. (*Middle*) Coomassie blue staining. (*Bottom*) RT-qPCR analysis of *NID1* expression relative to the parental cell line and normalized to *GAPDH* levels. (*H,I*) BLI quantification (*H*) and representative images (*I*) of lung metastasis by control and NID1 knockdown LM1a cell lines. *n* = 5–6. (*J*) Weights of primary tumors after subcutaneous injection of control and NID1 knockdown LM1a cell lines (at day 62 after injection). *n* = 8–12. Bar and whisker plots display the medians, 25th and 75th percent quartiles, and the full range of variation (from minimum to maximum). The *P*-value was calculated using the Mann-Whitney test. Data represent the mean ± SEM. (*) *P* < 0.05; (**) *P* < 0.01; (***) *P* < 0.001, Student's *t*-test.

early stage lung colonization. We first examined its role in cell migration and invasion, processes known to be important during metastasis and previously attributed to NID1 expression in endometrial cancer (Pedrola et al. 2015). Indeed, NID1 overexpression in MDA-MB-231 and HTB140 cells significantly increased transwell migration and invasion in modified Boyden chamber assays (Fig. 5A,B; Supplemental Fig. S7A,B), while knockdown in LM1a (Fig. 5C,D) and LM1-744 cells (Supplemental Fig. S7C,D) diminished these phenotypes in a manner dependent on the remaining NID1 levels (i.e., NID1-KD2 cells migrated and invaded at a slower rate than NID1-KD1 cells). Overall, our results suggest that NID1 modulates the migratory and invasive capabilities of breast cancer and melanoma cells, which may contribute toward an increased lung metastatic phenotype in vivo.

Next, we examined the role of NID1 in cell–cell and cell–matrix interactions, which facilitate early metastatic steps such as extravasation and adherence-dependent survival. The contribution of NID1 in the interaction of can-

cer cells with the microvascular endothelium, a key process for transendothelial migration during extravasation, was measured through cancer cell adhesion to monolayers formed by the human pulmonary microvascular EC line HPMEC-ST1.6R (Krump-Konvalinkova et al. 2001). NID1 overexpression in MDA-MB-231 (Fig. 5E), SCP28, and HTB140 cells (Supplemental Fig. S7E,F) significantly improved attachment by, on average, 50%. Conversely, knockdown of NID1 in LM1a and LM1-744 cells decreased attachment to the endothelium depending on knockdown efficacy, with NID1-KD2 exhibiting the lowest adherence ability (Supplemental Fig. S7G,H). Importantly, the adherence-promoting effect of NID1 was specific for adhesion to lung microvascular ECs, as overexpression of NID1 did not improve attachment to a monolayer formed by HPL1 lung epithelial cells or to plastic plates (Supplemental Fig. S7I).

To test whether the extracellular presence of NID1 is sufficient to account for the cell–cell adhesion phenotype, MDA-MB-231 and HTB140 cells were pretreated
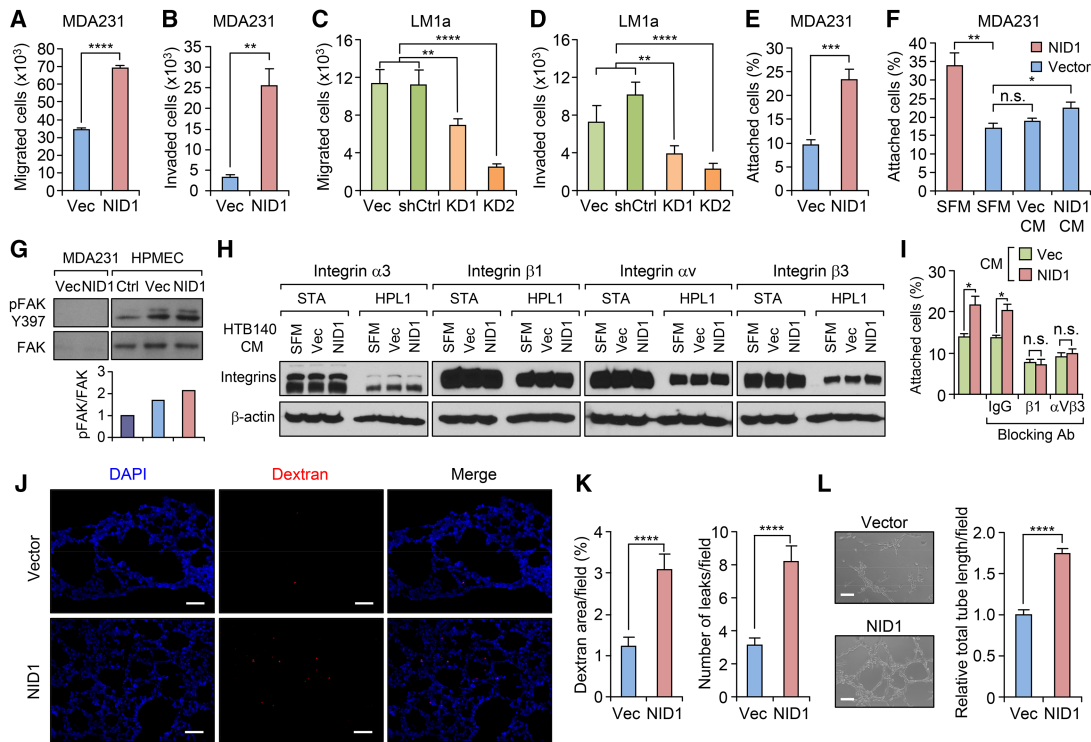
Figure 5. NID1 promotes cancer cell migration, invasion, adhesion to ECs, and tube formation in vitro. (*A,B*) Transwell migration (*A*) and invasion (*B*) assays of MDA-MB-231 vector and NID1-overexpressing cells. (*C,D*) Transwell migration (*C*) and invasion (*D*) assays of LM1a control (vector and scrambled shRNA) and NID1 knockdown (KD1 and KD2). (*E,F*) Attachment of vector or NID1-overexpressing MDA-MB-231 cells to HPMEC-ST1.6R EC monolayers. (*F*) Vector cells were pretreated with serum-free medium (SFM) or CM from vector or NID1-overexpressing MDA-MB-231 cells. (*G*) Western blot analysis of protein levels of focal adhesion kinase (FAK) and its phosphorylated form, pFAK Y397, in MDA-MB-231 vector control and NID1-overexpressing cells as well as ECs before and after incubation with cancer cells. Quantification of relative amounts of phosphorylated FAK (pFAK/FAK) in ECs is visualized; expression was normalized to the no cell control. (*H*) Western blot analysis of protein expression of integrin subunits α3, αv, β1, and β3 in ECs and HPL1 after incubation with CM from vector or NID1-overexpressing HTB140 cells. Expression of β-actin was used as a loading control. (*I*) Attachment of HTB140 cells to HPMEC-ST1.6R EC monolayers after pretreatment with CM from vector control and NID1-overexpressing HTB140 cells followed by treatment with various integrin-blocking antibodies, control IgG, or SFM. (*J,K*) Immunofluorescence images (*J*) and quantification (*K*) of vascular permeability by the area occupied by diffused dextran (*K, left*) and the number of leaked sites (*K, right*) after treatment of mice with CM derived from vector and NID1-overexpressing MDA-MB-231 cells. *n* = 10 mice. (*L*) Quantification and phase images of in vitro tube formation of MDA-MB-231 vector control and NID1 overexpression cells. Bar, 100 µm. In vitro assays were performed at least in triplicate. All data represent the mean ± SEM. (n.s.) Not significant; (*) *P* < 0.05; (**) *P* < 0.01; (***) *P* < 0.001; (****) *P* < 0.0001, Student's *t*-test.

with medium conditioned by NID1-overexpressing cells. This CM, but not CM from control cells, enhanced attachment to a confluent monolayer of ECs (Fig. 5F; Supplemental Fig. S7J). Thus, secreted NID1 may bind to the tumor cell surface and facilitate attachment to the endothelium by linking the cells or stabilizing their interaction.

Previous biochemical studies have identified integrins αvβ3 and α3β1 as NID1 receptors that facilitate cell binding to a NID1-containing ECM (Dedhar et al. 1992; Dong et al. 1995; Yi et al. 1998). We examined whether activation of integrin signaling through phosphorylation of the focal adhesion kinase (FAK) on Tyr397 (Y397) could be detected in the endothelium after cancer cell attachment. MDA-MB-231 cells used for attachment showed low basal FAK levels, while the presence of FAK and its phosphorylated form was higher in untreated HPMEC-ST1.6R

cells (Fig. 5G). Upon interaction with MDA-MB-231 cells, an increase in FAK phosphorylation in ECs was detected. Most importantly, ECs incubated with NID1-overexpressing cells showed enhanced FAK phosphorylation compared with coculture with vector control cells (Fig. 5G).

To address which integrin NID1 may bind to activate FAK phosphorylation, the expression of αvβ3 and α3β1 integrins in HPMEC-ST1.6R ECs was examined. Interestingly, all four integrin subunits examined were expressed in untreated and CM-treated ECs (Fig. 5H). Interestingly, all four integrin subunits, but particularly the α3 and β3 subunits, were expressed at much lower levels in HPL1 lung ECs, possibly explaining the lack of NID1-mediated increase in adhesion of cancer cells to HPL1 monolayers. More importantly, the functional significance of αvβ3 and α3β1 integrins in NID1-mediated enhancement of

cell adhesion was demonstrated using blocking antibodies against integrins β1 and αvβ3 (Fig. 5I). While inhibition of the β1 and αvβ3 integrins reduced adhesion of HTB140 melanoma cells to endothelial layers, it also eliminated the increase in adhesion facilitated by NID1-containing CM (Fig. 5I). This suggests that these integrins are needed for the NID1-mediated cancer cell attachment to endothelial layers. Surprisingly, a blocking antibody against the integrin α3 subunit promoted the adhesion of cancer cells to endothelial layers (data not shown), possibly due to effects unrelated to NID1 binding.

FAK activation in ECs has been shown to interfere with the stability of adherens junctions. We examined the involvement of NID1 in cancer cell-induced hyperpermeability of lung capillaries in vivo. Rhodamine-conjugated dextran was detected at significantly higher levels within lungs from mice inoculated with CM derived from NID1-overexpressing cells, as evidenced by the diffuse areas of fluorescence signal observed in lung sections (Fig. 5J,K; Supplemental Fig. 7K–M). This destabilization in pulmonary vasculature and increased permeability may facilitate exit of cancer cells from circulation. Indeed, NID1 overexpression in MDA-MB-231 cells increased migration through an EC monolayer (Supplemental Fig. S7N). In a similar way, at the physiological level of high NID1 expression by LM1-744 cells, a significantly higher level of permeability is observed in the lungs of the mice treated with LM1-744 CM compared with lungs from mice injected with parental HTB140 CM (Supplemental Fig. S7O–Q).

Last, we examined how NID1 affects the interaction of cancer cells with the surrounding ECM by culturing cells on top of Matrigel. All cancer cell lines exhibited tube formation capacity, a characteristic related to the vascular mimicry, a phenomenon that has been documented in highly aggressive tumor cells that express EC-associated genes and form perfusable, matrix-rich, and patterned tubular networks when cultured on a three-dimensional matrix (Maniotis et al. 1999). Vascular mimicry of tumor cells has been shown to promote metastatic outgrowth (Francescone et al. 2011; Wagenblast et al. 2015). NID1 overexpression promoted the tube formation capacity of breast cancer cell lines MDA-MB-231 and SCP28 as well as the melanoma HTB140 cell line (Fig. 5L; Supplemental Fig. S8A,B). Conversely, knockdown of NID1 in LM1a and LM1-744 cells significantly reduced the tube formation capability of melanoma cells (Supplemental Fig. S8C,D). In fact, knockdown cell lines, particularly NID1-KD2 with the lowest NID1 expression, formed clumps or cluster-like structures rather than tubes, a characteristic associated with a poor metastatic phenotype (Harrell et al. 2014). To evaluate whether extracellular NID1 was responsible for the observed phenotype, we incubated NID1-overexpressing cells with anti-NID1 antibody and observed a significant reduction in tube formation to the levels of control cells (Supplemental Fig. S8E). Taken together, these results indicate that extracellular NID1 facilitates the tube formation capability of cancer cells in vitro, thereby contributing toward a metastatic phenotype.

NID1 correlates with poor clinical outcome in breast cancer and melanoma patients

Given the functional importance of NID1 in promoting lung metastasis in mouse models, we explored whether NID1 expression has clinical significance as a prognostic marker in patient data sets. We first surveyed NID1 expression in breast cancer patients with and without metastasis in the EMC286-MSK cohorts (Minn et al. 2005; Wang et al. 2005) and found that while metastatic cancer patients displayed a trend toward higher NID1 levels compared with metastasis-free patients, those suffering from lung metastasis, but not bone metastasis, had significantly higher NID1 expression (Fig. 6A). In addition, we found that NID1 correlated with poor prognosis in multiple breast cancer clinical data sets (Fig. 6B–F). The KM Plotter database (Győrffy et al. 2010) showed that patients with high NID1 levels had an increased risk of developing distant metastasis (Fig. 6B–D), particularly among ER-negative patients (Fig. 6C). Moreover, using an independent patient cohort (NKI295) (van de Vijver et al. 2002), we confirmed that ER-negative patients exhibited shorter DMFS if NID1 expression was elevated (Fig. 6E), while no difference was observed among ER-positive patients (Fig. 6F). A similar analysis using the melanoma TCGA clinical microarray data set revealed that primary melanoma patients with high NID1 expression displayed shorter overall survival than those expressing lower levels (Fig. 6G). The 2-yr survival rate of patients with high expression of NID1 was 55.4%, compared with 80.3% for those with low expression. Taken together, NID1 is upregulated in breast cancer and melanoma patients with metastasis compared with metastasis-free patients and may predict poor prognosis in some cancer patient populations.

Discussion

Using a quantitative proteomic approach, we present comprehensive global and lung metastasis-specific secretome profiles derived from a well-established breast cancer model and a newly derived melanoma model of lung metastasis. These profiles demonstrate modest correlation of quantitative protein and mRNA measurements, highlighting the importance of protein level quantifications to avoid potential omission of metastasis markers or regulators, such as FN1 and NOV, in transcriptome-based profiling. The breast cancer-specific and melanoma-specific LMSSs, harboring many known and novel mediators and markers of lung metastasis, correlate with clinical outcome and lung relapse in multiple patient data sets. This indicates that LMSS proteins and their encoding genes, individually or as a signature, may be useful prognostic tools for assessing the risk for lung metastasis in clinical settings. The prognostic performance of LMSS proteins at the protein level, particularly as circulating biomarkers, needs to be assessed in future studies using patient samples because such noninvasive measurements not only are more convenient in the clinic but may also find stronger associations with clinical outcomes than
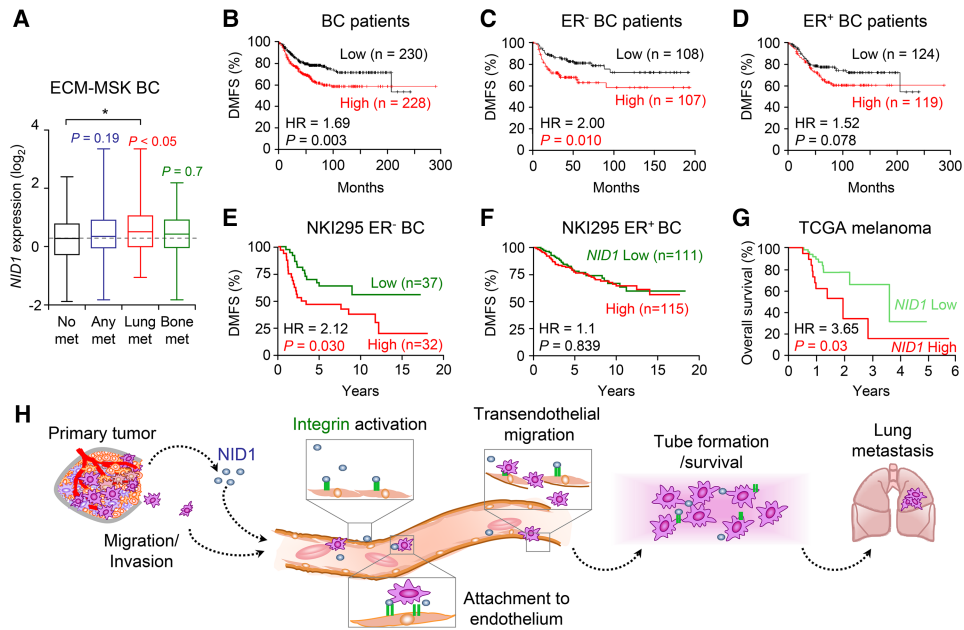
Figure 6. Clinical analysis of NID1 in patient data sets. (*A*) Box plot of *NID1* expression in samples from breast cancer patients who, at 30 mo after diagnosis, displayed no metastasis (No Met) or had metastasis (Any Met), including lung (Lung Met) and bone (Bone Met) metastasis. *P*-values are indicated *above* the corresponding box plots. (*B–D*) KM plot of DMFS of all (*B*), ER-negative (*C*), and ER-positive (*D*) grade 3 breast cancer patients, stratified by median primary tumor *NID1* expression (KM Plotter). $n = 458$ for all; $n = 215$ for ER⁻; $n = 243$ for ER⁺. (*E,F*) KM plot of DMFS of ER-negative (*E*) and ER-positive (*F*) breast cancer patients, stratified by median primary tumor *NID1* expression. NKI295, $n = 295$. (*G*) KM plot of overall survival of primary melanoma patients stratified by upper quartile primary tumor *NID1* expression. TCGA melanoma, $n = 470$. (*H*) Schematic representation of NID1 function during lung metastatic progression. Log-rank test *P*-values are displayed for KM plots. (*) $P < 0.05$, Student's *t*-test.

transcriptome-based analyses. In our study, we used transcriptomic data for clinical analyses due to a lack of such protein level data and hence we believe that the power of some of these markers may be underestimated. In support of this, several LMSS proteins have been reported previously as circulating biomarkers in cancer patients, correlating to presence of cancer or associating with poor clinical outcome. As such, serum CLIC4 levels were elevated in ovarian cancer patients compared with controls (Tang et al. 2013), LCP1 was increased in the plasma of patients with kidney cancer (Tang et al. 2013), and the plasma GDF15 levels were high in colorectal cancer patients and predicted poor survival (Wallin et al. 2011; Mehta et al. 2015).

Following the observation of increased NID1 secretion from aggressively lung metastatic breast cancer and melanoma cells, we experimentally validated NID1 as a novel promoter of lung metastasis in vivo and revealed its various metastasis-related functions in vitro. We demonstrated that NID1 enhances lung metastatic phenotypes by increasing migration, invasion, attachment to the endothelium, vascular permeability, and tube formation (Fig. 6H). Mechanistically, we demonstrated that NID1 activates integrin signaling in ECs, thereby disrupting intercellular junctions to enable transmigration of cancer cells and efficient extravasation into the lung parenchyma. The ability of NID1 to promote extravasation may promote general metastasis but is likely to be partic-

ularly important for facilitating lung metastasis compared with other distant sites. For instance, unlike bone sinusoids that have a discontinuous endothelium to facilitate the passage of hematopoietic and other cells (Oghiso and Matsuoka 1979), the lung contains a continuous endothelium with tight cell–cell junctions that requires a specialized ability of the metastatic tumor cells to promote vascular permeability and transendothelial migration in order to seed lung metastasis (Gupta et al. 2007; Padua et al. 2008). This is perhaps part of the reason why NID1 is specifically required for lung but not bone metastasis.

Clinically, high *NID1* expression correlates with lung relapse and poor prognosis in breast cancer and melanoma data sets. Tumor-derived NID1 may thus serve as a new biomarker for lung metastasis. In support of this, previous reports have shown elevated NID1 blood levels in multiple myeloma and ovarian cancer patients compared with healthy controls (Zhang et al. 2012; Khan et al. 2014; Li et al. 2015). Furthermore, high NID1 levels correlated with advanced stage and reflected tumor burden in ovarian cancer patients (Li et al. 2015). In future studies of NID1, serum or plasma levels will need to be assessed in breast cancer and melanoma patients, and association with lung relapse and clinical outcome will need to be correlated to examine its relevance as a blood biomarker.

NID1 has been shown to interact with other ECM proteins, including collagen, perlecan, and laminin (Chung and Durkin 1990; Fox et al. 1991; Dziadek 1995), thereby

facilitating ECM organization and basement membrane formation (Aumailley et al. 1993; Dziadek 1995; Tunggal et al. 2003). Previous studies have demonstrated that NID1-containing ECM promoted cancer cell attachment via interaction with cell surface integrins αvβ3 and α3β1 (Dedhar et al. 1992; Dong et al. 1995; Yi et al. 1998). Both αvβ3 and α3β1 integrins have also been implicated in later stages of metastasis, specifically during adhesion of circulating tumor cells to the vasculature (Felding-Habermann et al. 2001; Wang et al. 2004). Furthermore, α3β1 integrins expressed on circulating tumor cells have been shown to bind to laminin-5 within exposed regions of the vascular basement membrane during lung metastasis (Wang et al. 2004). Interestingly, integrin αvβ3, while not expressed on quiescent ECs, becomes markedly up-regulated at sites of angiogenesis and in response to human breast tumor cells (Brooks et al. 1995) and may facilitate cancer cell adhesion through interaction with tumor-derived NID1. In fact, phosphorylation of FAK, which can occur upon activation of integrin signaling, is elevated in ECs after binding to NID1-overexpressing cancer cells, supporting the hypothesis that cell adhesion is facilitated at least to some extent by NID1–integrin interactions. However, it is possible that other receptors and extracellular proteins that bind NID1 may also contribute to its lung metastasis-promoting functions. Notable interaction partners include PLXDC1/TEM7 (Lee et al. 2006), which is expressed in the human tumor endothelium (St Croix et al. 2000); the scavenger receptor LGALS3BP (Sasaki et al. 1998; Hellstern et al. 2002), which promotes integrin-mediated cell adhesion; and the putative cell adhesion receptor PTPRF/LAR (O'Grady et al. 1998).

Reminiscent of the role of TGFβ in cancer and metastatic progression, NID1 seems to be a tumor suppressor and metastasis promoter in our breast cancer and melanoma models. However, these functions may be cancer type-dependent, as NID1 promoted tumorigenesis and metastasis of endometrial cancer (Pedrola et al. 2015), while loss of expression through promoter methylation in colon and gastric cancers (Ulazzi et al. 2007) or increased protein degradation in prostate cancer (Ko et al. 2015) correlated with enhanced tumor growth and metastasis. One possible mechanism by which NID1 may decrease tumorigenesis could be its strong binding affinity for perlecan, which can be secreted by quiescent ECs to mute proliferative and invasive phenotypes of lung and breast cancer cells in vitro and reduce their protumorigenic and proinflammatory signaling (Franses et al. 2011).

Overall, we provide a valuable resource of lung metastasis secretomes in breast cancer and melanoma, which contains known and putative mediators and markers of lung metastasis. Our study highlights the importance of analyzing secreted proteins on a proteomic-level to understand complex tumor–stroma interactions at distant sites. We also experimentally validate the novel role of NID1 in promoting lung metastasis of breast cancer and melanoma by enhancing several prometastatic characteristics, including cell migration, attachment to an endothelium, vascular permeability, and tube formation. As NID1 is a secreted protein that is easily accessible to inhibitors,

new therapeutic methods may be developed to specifically target NID1 for reducing lung metastasis.

Materials and methods

Cell lines, cell sorting, and isolation of lung metastatic sublines

The breast cancer cell line MDA-MB-231 was obtained from American Type Culture Collection (ATCC), while its sublines, LM2-A and LM2-B, were kindly provided by Dr. J. Massagué (Memorial Sloan Kettering Cancer Center). All breast cancer cell lines were maintained in Dulbecco's modified Eagle's medium (DMEM) (Coring) supplemented with 10% heat-inactivated fetal bovine serum (FBS) (Gemini), penicillin/streptomycin (Coring), and amphotericin B (Coring) unless otherwise noted. HTB140 (obtained from ATTC) and its sublines, including LM1a and LM1-744, were supplemented with 10% not heat-inactivated FBS (Gemini), penicillin/streptomycin (Coring), and amphotericin B (Coring) unless otherwise noted. The HPMEC-ST1.6R human pulmonary microvascular EC line (Krump-Konvalinkova et al. 2001) was cultured in M199 medium (Gibco) supplemented with 20% heat-inactivated FBS, 50 μg/mL ECGS, penicillin/streptomycin (Gibco), and amphotericin B. The human epithelial cell line HPL1 was cultured as described previously (Masuda et al. 1997).

All cell lines used in this study were tested regularly on a monthly basis for mycoplasma throughout the study, and results were consistently negative. Mycoplasma testing was performed as described previously (Uphoff and Drexler 2011). The Genetica STR profiling service was used to determine the STR profiles of the six cell lines used in the secretome analysis. The STR profiles were matched to the ATCC STR database (https://www.atcc.org/STR%20Database.aspx) and confirmed the authentication of these cell lines (Supplemental Table S10).

For bioluminescent tracking, cell lines were retrovirally infected with a triple-fusion protein reporter construct encoding herpes simplex virus thymidine kinase 1, green fluorescent protein (GFP), and firefly luciferase (Kang et al. 2003). GFP-positive cells were enriched by fluorescence-activated cell sorting (FACS).

To isolate lung metastatic sublines from lung lesions using the parental HTB140 melanoma cell line, BALB/c nude mice were injected with 10^6 HTB140 luciferase-labeled cells by tail vein injection and allowed to develop lung metastases. Metastatic progression was monitored by weekly bioluminescence imaging (BLI). At the experimental end points, lungs were harvested, and single lung metastatic nodules were isolated and dissociated mechanically. Cells were collected by centrifugation and washed once with PBS before being cultured in 5-cm plates using regular HTB140 culture medium. After cells reached confluence, they were sorted by FACS based on GFP expression to isolate a pure population of human melanoma cells. Each newly derived lung metastatic subline was obtained from a single lung metastatic nodule.

CM preparation

For quantitative SILAC analyses, matched pairs of highly or lowly lung metastatic cell lines were cultured in DMEM without arginine and lysine supplemented with 10% dialyzed FBS (Invitrogen) and either normal or heavy arginine (13C6, 15N4; +10 Da) (Thermo Scientific Pierce) and lysine (13C6, 15N2; +8 Da) (Sigma). After 7 d of culture, cells were counted, and equal numbers of cells were split into 15-cm dishes at ~50% confluence. Once cell lines reached ~70% confluence, two 15-cm dishes of each cell line were washed three times with PBS to remove serum

proteins and incubated for 24 h in 15 mL of serum-free DMEM. CM was then removed, mixed, filtered with 0.45-μm filters, and maximally concentrated (75-fold to 100-fold) via centrifugation at 4000 rpm at room temperature in 3-kDa molecular weight cutoff (MWCO) concentrating columns (Millipore). Concentrated CM samples were stored at −80°C until processing for MS.

For NID1-related experiments, CM was prepared similarly to as described above. Briefly, once cells reached ∼80% confluence, plates were washed three times with PBS and incubated with serum-free medium (SFM) for 24 h. CM was collected and centrifuged at 1000 rpm for 5 min or filtered using a 0.45-μm filter to remove any cells or cell debris. CM was concentrated using MWCO columns of 50 or 100 kDa (Amicon) to obtain ∼10-fold concentrated medium.

Sample preparation and MS

Samples for MS analysis were prepared as described previously (Blanco et al. 2012). Briefly, concentrated CM samples were run on 10% SDS–polyacrylamide gels and cut into 12 gel slices per sample. Solubilized gel slices were treated with dithiothreitol and iodoacetamide prior to in-gel digestion with trypsin at a 20:1 protein:enzyme ratio for 12 h at 37°C (Shevchenko et al. 1996). All peptide digests were desalted using homemade C_{18} STAGE tips (Rappsilber et al. 2003), dried to near dryness in a vacuum centrifuge, and diluted in 10 μL of 0.1% acetic acid for MS analysis.

MS was performed as described previously (LeRoy et al. 2009; Blanco et al. 2012). Briefly, nanoflow liquid chromatography MS/MS (nLC-MS/MS) was performed on a hybrid linear ion trap Orbitrap mass spectrometer (Thermo Electron) coupled to an Agilent 1200 series binary high-performance liquid chromatography (HPLC) pump (Agilent Technologies) and an Eksigent AS2 autosampler (Eksigent Technologies). Peptides samples (2 μL) were loaded onto 75-μm inner diameter fused silica capillary columns constructed with integrated electrospray tips that were packed with 15 cm of C_{18} reversed-phase (RP) resin (Magic C18, 5-μm particles, 200-Å pore size; Michrom BioResources). Peptides were separated by RP-HPLC using a gradient from 2% to 45% buffer B (buffer A: 0.1% acetic acid; buffer B: 70% acetonitrile in 0.1% acetic acid) at a flow rate of ∼200 nL/min for 110 min. The Orbitrap instrument was operated in data-dependent mode using a resolution setting of 30,000 to obtain a full MS spectrum followed by 10 MS/MS spectra obtained in the ion trap. Peptides selected for MS/MS fragmentation were then placed on an exclusion list for 30 sec to limit duplicate spectra. The MS scans were collected with an automatic gain control target value of 5×10^5 and maximum injection time of 100 msec over a mass range of 300–1650 m/z. MS/MS scans were collected using an automatic gain control value of 4×10^4 and threshold energy of 35% for collision-activated dissociation.

MS data analysis

All MS/MS spectra were processed through the MaxQuant program (Franses et al. 2011). Parameters for MS/MS database searching included the following: precursor mass tolerance, 4.5 ppm; product mass tolerance, 0.5 Da; enzyme, trypsin; missed cleavages allowed, two; static modifications, carbamidomethyl (C); variable modifications, acetyl (protein N-terminal) and oxidation (M); and database, *Homo sapiens* (UniProt, July 2014). PSMs and protein false discovery rate were filtered for <0.01. Data were log-transformed and normalized, and statistics were assessed using the t-test (homoscedastic; two independent samples). All MS proteomics data were deposited at The Chorus Project (https://chorusproject.org) with ID number 1046.

Subcellular compartment and GO enrichment analyses

Annotation of extracellular proteins was performed manually using the European Bioinformatics Institute (EMBL-EBI) UniProt Gene Ontology Annotation database (Huntley et al. 2015) in the QuickGO software (Binns et al. 2009), ExoCarta (Mathivanan and Simpson 2009), and Vesiclepedia (Kalra et al. 2012). The human GO annotation "extracellular region" (GO: 0005576) was extracted from QuickGO (latest update November 1, 2015), and proteins found within this ontology were annotated as extracellular. Proteins were further probed for the presence in the child terms "extracellular exosome compartment" (GO: 0070062) and "external side of the plasma membrane" (GO:0009897) within this data set. Proteins were annotated as exosomal if found within the ExoCarta (version 5) and Vesiclepedia (version 3) data sets at the protein level and in human samples only.

For GO enrichment analysis, proteins were subjected to BiNGO analysis (version 3.0.3) (Maere et al. 2005) using Cytoscape software version 3.2.1 (Lotia et al. 2013). Parameters were set to show overrepresentation of GO terms with P-values <0.05 (hygrometric statistical test with Benjamin and Hochberg false discovery rate [FDR] correction). GOSlim GOA, representing a subset of the broadest GO terms, and GO FAT ontology files, in which the broadest terms were excluded in order to not overshadow more specific terms, were interrogated for GO enrichment analysis of all proteins. GO FAT ontologies were obtained from DAVID (Huang et al. 2008), and redundant and child terms were removed using Reduce and Visualize GO (REViGO) (Supek et al. 2011) and manual inspection and visualized using Cytoscape. For LMSSs, GO Biological Process and GO Molecular Function ontologies were interrogated. For all analyses, annotations with five or fewer proteins were excluded.

Protein interaction network analysis

To analyze the interactome of the lung metastatic secretome from breast cancer and melanoma, the cancer-specific Up-LMSSs and Down-LMSSs were combined and imported into STRING (version 10) (Szklarczyk et al. 2015). Protein interactions were mapped by displaying only high-confidence interactions with a score of 0.7. The networks were downloaded and then processed using Cytoscape (Lotia et al. 2013). Clustering into protein families and functional categories was performed manually.

Analysis for association with survival and incidence/sites of metastasis

For clinical data set survival analyses, association between gene expression and metastasis was assessed using a univariate Cox proportional hazards model or KM estimator provided by the online KM Plotter database (version 2014) (Györffy et al. 2010). Significance of survival differences between groups was assessed by log-rank test, with $P < 0.05$ being considered significant. For breast cancer signature analyses, the multigene classifier option on KM Plotter was used to analyze the mean expression of the top 40 genes in each signature and correlate it with DMFS. An upper quartile cutoff was used for the Up-LMSS, and a lower quartile cutoff was used for the Down-LMSS. At the time of analysis, 664 breast cancer patients were included in the analysis, among which 227 were ER-negative and 437 were ER-positive. For melanoma signature analysis, a score based on the sum of the Z-scores for each of the top 40 genes was calculated for the 470 patients in the TCGA skin cutaneous melanoma data set (http://cancergenome.nih.gov). Patients were then stratified by the median score, and the overall survival was assessed. The KM Plotter database was used to assess the correlation between *NID1* expression and DMFS in grade 3 breast cancer patients using a median

cutoff. KM estimators were used to predict DMFS in the NKI295 data set (van de Vijver et al. 2002), stratified into high and low *NID1* expression groups based on median expression. To assess association with incidence/sites of metastasis, tumors collected on the EMC286-MSK (Minn et al. 2005; Wang et al. 2005) and TCGA melanoma data sets were grouped according to incidence and/or site of metastasis, and differences in group expression means were assessed by two-sided Student's *t*-tests with the assumption of equal variance. The survival analysis of melanoma patients was done using Matlab. The Matlab code is provided as both a ".m" file (Supplemental File 1), which is the format for Matlab, and a ".txt" file (Supplemental File 2). The TCGA melanoma clinical data set is provided as an Excel file (Supplemental Table S11) and is needed to run the program, as the program imports data from the sheet.

For the EMC286-MSK data set, groups were defined based on whether metastasis occurred at 30 mo. GSEA version 2.0 (Subramanian et al. 2005) was used to determine enrichment of lung metastasis signatures in the normalized microarray data of the published clinical data set EMC286 (Wang et al. 2005) after it was separated into metastasis-free and either general or site-specific metastasis phenotypes. For gene list ranking, multiple probe matches were collapsed into one value, with the highest probe reading being used in each case. Only probes with matches to gene symbols were used. Genes were ranked using the provided signal to noise ranking statistic, and GSEA was run using a weighted statistic and elevated for statistical significance by comparison with results obtained using 1000 random permutations of each gene set. For all other GSEA parameters, default settings were used.

Western blot analysis

For Western blot analysis, whole-cell lysate and CM samples were subjected to SDS-PAGE and subsequently transferred to Immobilon PVDF membranes (Millipore). Membranes were blocked in 5% milk for 1 h prior to overnight primary antibody incubation. The primary antibodies used were anit-NID1 (1:1000; Abcam, ab133686), anti-FAK and anti-phospho-FAK (Tyr397) (1:1000; Cell Signaling Technology FAK antibody sampler kit, 9330), anti-integrin β1 antibody (EP1041Y) (1:1000; Abcam, ab52971), anti-integrin αV antibody (EPR16800) (1:5000; Abcam, ab179475), anti-integrin β3 antibody (EPR2342) (1:1000; Abcam, ab119992), and anti-integrin α3 antibody (1:1000; Abcam, ab190731). Membranes were incubated with horseradish peroxidase (HRP)-conjugated anti-mouse secondary antibody (1:2000 dilution; GE Healthcare) or anti-rabbit secondary antibody (1:2000 dilution; GE Healthcare) for 1 h, and chemiluminescence signals were detected by ECL substrate (GE Healthcare). Coomassie blue staining of the membrane was used to assess equal loading of CM samples. Gel quantifications were performed using ImageJ (National Institutes of Health).

Reverse transcription and RT-qPCR

Total RNA was isolated using the RNeasy kit (Qiagen) and reverse-transcribed with the SuperScript III kit (Invitrogen) following the manufacturer's instructions. RT-qPCR was performed using the SYBR Green PCR Master mix (Applied Biosystems) with an ABI Prism 7900HT thermocycler (Applied Biosystems).

Generation of stable cell lines

Stable overexpression of all genes was achieved using the pLEX lentiviral plasmid. Lentiviral vectors were transfected into the packaging cell line HEK293T. After 48 h, viruses were collected, filtered, concentrated, and used to infect target cells in the presence of 8 μg/mL polybrene. The infected cells were selected with puromycin. Stable shRNA-mediated knockdown was achieved with the MISSION lentivirus system (Sigma).

Transwell migration, invasion, and transendothelial migration assays

Migration and invasion were performed as described previously (Korpal et al. 2011). Briefly, cancer cells were scraped off plates, washed in PBS, and resuspended in SFM. Cells (10^5) were placed in inserts (Costar) containing 8-μm pores coated with (invasion assay) or without (migration assay) 1 mg/mL Matrigel. Inserts were then placed in wells with regular medium. Twelve hours (migration) or 24 h (invasion) after seeding, regular medium was collected, and 500 μL of trypsin was added to the wells to trypsinize cells that had passed through the pores. Trypsin was neutralized with the collected regular medium and centrifuged for 5 min at 1000 rpm. The medium was aspirated to leave ∼100 μL for resuspension of the cell pellet. The remaining volume was recorded, and 10 μL of resuspended cells was used to count the total number of cells that had migrated through the pores using a hemocytometer. For transendothelial migration assays, Matrigel-precoated inserts were seeded with 10^5 HPMEC-ST1.6R cells and incubated in HPMEC-ST1.6R medium to allow for the formation of a confluent EC monolayer. Cancer cells were seeded onto EC monolayers in FBS-reduced HPMEC-ST1.6R medium (2.5% FBS) and incubated for 12 h. Cells were harvested as described above, lysed with luciferase lysis buffer (2 mM EDT, 20 mM DTT, 10% glycerol, 1% Triton X-100, 25 mM Tris at pH 7.8), and quantified by firefly luciferase assay. Mean signal intensity calculated from at least five technical replicates of each condition was normalized to luminescence from control wells containing the starting number of cancer cells that were plated in parallel.

Endothelial adhesion assay

To test the adhesion of cancer cells to the ECs, the HPMEC-ST1.6R EC line was grown to confluence in a 24-well plate. Once confluent, the monolayers were pretreated with 1× CM (diluted 10-fold from 10× concentrated CM) for 24 h before the adhesion assay was performed. Luciferase-labeled cancer cells were scraped off plates, washed in PBS, and resuspended in cell attachment buffer (HPMEC-ST1.6R medium supplemented with 1 mM $CaCl_2$, 1 mM $MnCl_2$, and 1 mM $MgCl_2$). Cells (5×10^4) were seeded onto the EC monolayer in a total volume of 1 mL or less and incubated for 30 min at 37°C. The same number of cells was added to three Eppendorf tubes to be used as total cell number controls and for normalization. Unbound cells were removed by washing three times with PBS. Attached cells were lysed with luciferase lysis buffer and quantified by firefly luciferase assay using GloMax. The luminescence intensity of each well was normalized to that of lysed added cells from the Eppendorf tubes. For pretreatment studies, CM was collected, filtered through a 0.2-μm filter, and concentrated using a filter unit (100 kDa MWCO; Amicon). Cells were pretreated with concentrated CM for 24 h before adhesion assays.

For blocking experiments with antibodies against different integrin subunits, the following antibodies were used: anti-integrin α3 (clone ASC-1; Sigma, MAB2056Z), anti-integrin β1 (clone P5D2; R&D, MAB17781), and anti-integrin αVβ3 (clone 23C6; Thermo Fisher, 16-0519-81). IgG controls were from Thermo Fisher. HPMEC-ST1.6R cells were seeded into wells of gelatin-treated white 96-well plates and grown to confluency. Confluency was determined by observing cells in transparent plates seeded in parallel. Prior to the adhesion assay, ECs were

treated with CM from vector control and NID1-overexpressing HTB140 cells overnight. The next day, integrin-blocking antibodies and controls (IgG and PBS) were resuspended in cell attachment buffer containing the corresponding 1× CM at a concentration of 10 µg/mL. Fifty microliters of the antibody–CM mixture was added per well and incubated for 20 min. Luciferase-labeled HTB140 cells (1.5×10^4 cells) were suspended in binding medium containing 1× CM. The cells were gently added in a volume of 50 µL per well to the pretreated wells on top of integrin-blocking antibodies. Cells were incubated for 40 min at 37°C and then gently removed and washed three times with DPBS using a multichannel pipet. One-hundred microliters of EC medium followed by 50 µL of 1 µg/mL D-luciferin in DPBS was added to the wells, and luciferase activity was determined using GloMax. Wells that were seeded in parallel but not washed were used as the control for total seeding and to calculate the adhesion percentage.

Vascular permeability assay

Lung microvasculature permeability was determined by the rhodamine–dextran extravasation technique. Mice were injected intravenously with 100 µL of 10× CM for two consecutive days. On the second day, mice were injected intravenously with rhodamine-conjugated dextran 70,000 MW at 1 mg per 20 g of body weight followed by anesthesia exactly 1 h later. Lungs were heart-perfused with PBS, dissected, and fixed in 2% PFA with 20% sucrose. Eight-micrometer cryosections of lungs were stained with DAPI and examined by fluorescence microscopy for vascular leakage. ImageJ was used to quantify individual sites of leakage and percentage area of perfused dextran. Images of the red (rhodamine–dextran) channel were first converted to a binary image, and a fixed threshold was applied. Images were then subjected to the "Analyze Particles" analysis with settings for sizes of 10 to infinity. Counts were used as a quantification of individual sites of leakage, while %area was used as a quantification for the percentage area of perfused dextran.

Tube formation assay

Ninety-six-well plates were coated with 50 µL of growth factor-reduced Matrigel (BD Biosciences), and 10^4 to 10^5 cells were plated with SFM in each well as described previously (Francescone et al. 2011). For antibody treatments, cells were incubated with 1 mg/mL anti-NID1 antibody for 30 min at 4°C prior to seeding. All cells were plated in at least four replicates. Morphology studies were performed 2–24 h after seeding, depending on the cell line, using the Zeiss Axiovert 200 microscope and AxioVision software version 4.6.3 SP1. Tube formation was quantified using the Angiogenesis Analyzer plug-in in ImageJ (http://http://image.bio.methods.free.fr/ImageJ/?Angiogenesis-Analyzer-for-ImageJ).

Tumor xenografts, bioluminescence, and histological analyses

All animal work was performed in accordance with the guidelines of the Institutional Animal Care and Use Committee of Princeton University under approved protocols. For lung metastasis experiments, 1×10^5 luciferase-labeled cancer cells were washed in PBS and injected via tail vein into 6- to 8-wk-old female athymic nude (breast cancer cell lines) or male NSG (melanoma cell lines) mice. Noninvasive bioluminescent imaging was performed to quantify the metastasis burden in using an IVIS 200 imaging system (Caliper Life Sciences). Analysis was performed with Living Image software (Xenogen) by measuring photon flux of the region of interest. Data were normalized to the signal obtained immedi-

ately after injection (day 0). For primary tumor experiments, 1×10^5 cancer cells were injected into the mammary fat pad (breast cancer) or subcutaneously (melanoma). Tumor size was measured weekly using a caliper, and volume was calculated using the formula width^2 × length/2. At the end point, tumors were excised, and tumor weight was determined using a scale.

Statistics and bioinformatics

For statistical analyses, results were reported as average ± SEM. Two-sided independent Student's *t*-tests without equal variance assumption were performed to analyze data from in vitro assays and in vivo experiments. In each statistical analysis, $P < 0.05$ was considered statistically significant. Bar and whisker plots display the medians, 25th and 75th percent quartiles, and the full range of variation (from minimum to maximum). The *P*-value was calculated using the Mann-Whitney test.

Acknowledgments

References

Akiyama S, Olden K, Yamada K. 1995. Fibronectin and integrins in invasion and metastasis. *Cancer Metastasis Rev* **14:** 173–189.

Alečković M, Kang Y. 2015. Regulation of cancer metastasis by cell-free miRNAs. *Biochim Biophys Acta* **1855:** 24–42.

Aumailley M, Battaglia C, Mayer U, Reinhardt D, Nischt R, Timpl R, Fox JW. 1993. Nidogen mediates the formation of ternary complexes of basement membrane components. *Kidney Int* **43:** 7–12.

Benini S, Perbal B, Zambelli D, Colombo MP, Manara MC, Serra M, Parenza M, Martinez V, Picci P, Scotlandi K. 2005. In Ewing's sarcoma CCN3(NOV) inhibits proliferation while promoting migration and invasion of the same cell type. *Oncogene* **24:** 4349–4361.

Binns D, Dimmer E, Huntley R, Barrell D, O'Donovan C, Apweiler R. 2009. QuickGO: a Web-based tool for gene ontology searching. *Bioinformatics* **25:** 3045–3046.

Blanco MA, LeRoy G, Khan Z, Aleckovic M, Zee BM, Garcia BA, Kang Y. 2012. Global secretome analysis identifies novel mediators of bone metastasis. *Cell Res* **22:** 1339–1355.

Bosserhoff AK, Buettner R. 2002. Expression, function and clinical relevance of MIA (melanoma inhibitory activity). *Histol Histopathol* **7:** 289–300.

Brooks PC, Strömblad S, Klemke R, Visscher D, Sarkar FH, Cheresh DA. 1995. Antiintegrin αvβ3 blocks human breast cancer growth and angiogenesis in human skin. *J Clin Invest* **96:** 1815–1822.

Chung AE, Durkin ME. 1990. Entactin: structure and function. *Am J Respir Cell Mol Biol* **3:** 275–282.

Dedhar S, Jewell K, Rojiani M, Gray V. 1992. The receptor for the basement membrane glycoprotein entactin is the integrin α3/β1. *J Biol Chem* **267.**

Dong LJ, Hsieh JC, Chung AE. 1995. Two distinct cell attachment sites in entactin are revealed by amino acid substitutions and

deletion of the RGD sequence in the cysteine-rich epidermal growth factor repeat 2. *J Biol Chem* **270:** 15838–15843.

Dziadek M. 1995. Role of laminin-nidogen complexes in basement membrane formation during embryonic development. *Experientia* **51:** 901–913.

Ell B, Kang Y. 2012. SnapShot: bone metastasis. *Cell* **151:** 690–690.e691.

Erler JT, Bennewith KL, Nicolau M, Dornhofer N, Kong C, Le Q-T, Chi J-TA, Jeffrey SS, Giaccia AJ. 2006. Lysyl oxidase is essential for hypoxia-induced metastasis. *Nature* **440:** 1222–1226.

Felding-Habermann B, O'Toole TE, Smith JW, Fransvea E, Ruggeri ZM, Ginsberg MH, Hughes PE, Pampori N, Shattil SJ, Saven A, et al. 2001. Integrin activation controls metastasis in human breast cancer. *Proc Natl Acad Sci* **98:** 1853–1858.

Fernandez-Garcia B, Eiró N, Marín L, González-Reyes S, González LO, Lamelas ML, Vizoso FJ. 2014. Expression and prognostic significance of fibronectin and matrix metalloproteases in breast cancer metastasis. *Histopathology* **64:** 512–522.

Fogh J, Fogh JM, Orfeo T. 1977. One hundred and twenty-seven cultured human tumor cell lines producing tumors in nude mice. *J Natl Cancer Inst* **59:** 221–226.

Fox JW, Mayer U, Nischt R, Aumailley M, Reinhardt D, Wiedemann H, Mann K, Timpl R, Krieg T, Engel J. 1991. Recombinant nidogen consists of three globular domains and mediates binding of laminin to collagen type IV. *EMBO J* **10:** 3137–3146.

Francescone RA III, Faibish M, Shao R. 2011. A Matrigel-based tube formation assay to assess the vasculogenic activity of tumor cells. *J Vis Exp* 3040.

Franses JW, Baker AB, Chitalia VC, Edelman ER. 2011. Stromal endothelial cells directly influence cancer progression. *Sci Transl Med* **3:** 66ra65.

Futreal PA, Coin L, Marshall M, Down T, Hubbard T, Wooster R, Rahman N, Stratton MR. 2004. A census of human cancer genes. *Nat Rev Cancer* **4:** 177–183.

Glukhova L, Angevin E, Lavialle C, Cadot B, Terrier-Lacombe M-J, Perbal B, Bernheim A, Goguel A-F. 2001. Patterns of specific genomic alterations associated with poor prognosis in high-grade renal cell carcinomas. *Cancer Genet Cytogenet* **130:** 105–110.

Gupta GP, Nguyen DX, Chiang AC, Bos PD, Kim JY, Nadal C, Gomis RR, Manova-Todorova K, Massague J. 2007. Mediators of vascular remodelling co-opted for sequential steps in lung metastasis. *Nature* **446:** 765–770.

Györffy B, Lanczky A, Eklund A, Denkert C, Budczies J, Li Q, Szallasi Z. 2010. An online survival analysis tool to rapidly assess the effect of 22,277 genes on breast cancer prognosis using microarray data of 1,809 patients. *Breast Cancer Res Treat* **123:** 725–731.

Harrell JC, Pfefferle AD, Zalles N, Prat A, Fan C, Khramtsov A, Olopade OI, Troester MA, Dudley AC, Perou CM. 2014. Endothelial-like properties of claudin-low breast cancer cells promote tumor vascular permeability and metastasis. *Clin Exp Metastasis* **31:** 33–45.

Hellstern S, Sasaki T, Fauser C, Lustig A, Timpl R, Engel J. 2002. Functional studies on recombinant domains of Mac-2-binding protein. *J Biol Chem* **277:** 15690–15696.

Huang DW, Sherman BT, Lempicki RA. 2008. Systematic and integrative analysis of large gene lists using DAVID bioinformatics resources. *Nat Protoc* **4:** 44–57.

Huntley RP, Sawford T, Mutowo-Meullenet P, Shypitsyna A, Bonilla C, Martin MJ, O'Donovan C. 2015. The GOA database: gene ontology annotation updates for 2015. *Nucleic Acids Res* **43:** D1057–D1063.

Jin L, Zhang Y, Li H, Yao L, Fu D, Yao X, Xu LX, Hu X, Hu G. 2012. Differential secretome analysis reveals CST6 as a suppressor of breast cancer bone metastasis. *Cell Res* **22:** 1356–1373.

Kalra H, Simpson RJ, Ji H, Aikawa E, Altevogt P, Askenase P, Bond VC, Borràs FE, Breakefield X, Budnik V, et al. 2012. Vesiclepedia: a compendium for extracellular vesicles with continuous community annotation. *PLoS Biol* **10:** e1001450.

Kang Y, Siegel PM, Shu W, Drobnjak M, Kakonen SM, Cordon-Cardo C, Guise TA, Massague J. 2003. A multigenic program mediating breast cancer metastasis to bone. *Cancer Cell* **3:** 537–549.

Kaplan RN, Riba RD, Zacharoulis S, Bramley AH, Vincent L, Costa C, MacDonald DD, Jin DK, Shido K, Kerns SA, et al. 2005. VEGFR1-positive haematopoietic bone marrow progenitors initiate the pre-metastatic niche. *Nature* **438:** 820–827.

Khan R, Gupta N, Kumar R, Sharma M, Kumar L, Sharma A. 2014. Augmented expression of urokinase plasminogen activator and extracellular matrix proteins associates with multiple myeloma progression. *Clin Exp Metastasis* **31:** 585–593.

Ko C-J, Huang C-C, Lin H-Y, Juan C-P, Lan S-W, Shyu H-Y, Wu S-R, Hsiao P-W, Huang H-P, Shun C-T, et al. 2015. Androgen-induced TMPRSS2 activates matriptase and promotes extracellular matrix degradation, prostate cancer cell invasion, tumor growth, and metastasis. *Cancer Res* **75:** 2949–2960.

Korpal M, Ell BJ, Buffa FM, Ibrahim T, Blanco MA, Celià-Terrassa T, Mercatali L, Khan Z, Goodarzi H, Hua Y, et al. 2011. Direct targeting of Sec23a by miR-200s influences cancer cell secretome and promotes metastatic colonization. *Nat Med* **17:** 1101–1108.

Krump-Konvalinkova V, Bittinger F, Unger RE, Peters K, Lehr HA, Kirkpatrick CJ. 2001. Generation of human pulmonary microvascular endothelial cell lines. *Lab Invest* **81:** 1717–1727.

Lee HK, Seo IA, Park HK, Park HT. 2006. Identification of the basement membrane protein nidogen as a candidate ligand for tumor endothelial marker 7 in vitro and in vivo. *FEBS Lett* **580:** 2253–2257.

Lee SB, Schramme A, Doberstein K, Dummer R, Abdel-Bakky MS, Keller S, Altevogt P, Oh ST, Reichrath J, Oxmann D, et al. 2010. ADAM10 is upregulated in melanoma metastasis compared with primary melanoma. *J Invest Dermatol* **130:** 763–773.

LeRoy G, Weston JT, Zee BM, Young NL, Plazas-Mayorca MD, Garcia BA. 2009. Heterochromatin protein 1 is extensively decorated with histone code-like post-translational modifications. *Mol Cell Proteomics* **8:** 2432–2442.

Li L, Zhang Y, Li N, Feng L, Yao H, Zhang R, Li B, Li X, Han N, Gao Y, et al. 2015. Nidogen-1: a candidate biomarker for ovarian serous cancer. *Jpn J Clin Oncol* **45:** 176–182.

Liu S, Han L, Wang X, Liu Z, Ding S, Lu J, Bi D, Niu Z. 2015. Nephroblastoma overexpressed gene (NOV) enhances RCC cell motility through upregulation of ICAM-1 and COX-2 expression via Akt pathway. *Int J Clin Exp Pathol* **8:** 1302–1311.

Lotia S, Montojo J, Dong Y, Bader GD, Pico AR. 2013. Cytoscape App Store. *Bioinformatics* **29:** 1350–1351.

Maere S, Heymans K, Kuiper M. 2005. BiNGO: a Cytoscape plugin to assess overrepresentation of gene ontology categories in Biological Networks. *Bioinformatics* **21:** 3448–3449.

Malik G, Knowles LM, Dhir R, Xu S, Yang S, Ruoslahti E, Pilch J. 2010. Plasma fibronectin promotes lung metastasis by contributions to fibrin clots and tumor cell invasion. *Cancer Res* **70:** 4327–4334.

Maniotis AJ, Folberg R, Hess A, Seftor EA, Gardner LM, Pe'er J, Trent JM, Meltzer PS, Hendrix MJ. 1999. Vascular channel

formation by human melanoma cells in vivo and in vitro: vasculogenic mimicry. *Am J Pathol* **155:** 739–752.

Maric G, Rose AAN, Annis MG, Siegel PM. 2013. Glycoprotein non-metastatic b (GPNMB): a metastatic mediator and emerging therapeutic target in cancer. *Onco Targets Ther* **6:** 839–852.

Masuda A, Kondo M, Saito T, Yatabe Y, Kobayashi T, Okamoto M, Suyama M, Takahashi T. 1997. Establishment of human peripheral lung epithelial cell lines (HPL1) retaining differentiated characteristics and responsiveness to epidermal growth factor, hepatocyte growth factor, and transforming growth factor β1. *Cancer Res* **57:** 4898–4904.

Mathivanan S, Simpson RJ. 2009. ExoCarta: a compendium of exosomal proteins and RNA. *Proteomics* **9:** 4997–5000.

Mehta RS, Chong DQ, Song M, Meyerhardt JA, Ng K, Nishihara R, Qian Z, Morikawa T, Wu K, Giovannucci EL, et al. 2015. Association between plasma levels of macrophage inhibitory cytokine-1 before diagnosis of colorectal cancer and mortality. *Gastroenterology* **149:** 614–622.

Minn AJ, Gupta GP, Siegel PM, Bos PD, Shu W, Giri DD, Viale A, Olshen AB, Gerald WL, Massague J. 2005. Genes that mediate breast cancer metastasis to lung. *Nature* **436:** 518–524.

Naba A, Clauser KR, Lamar JM, Carr SA, Hynes RO. 2014a. Extracellular matrix signatures of human mammary carcinoma identify novel metastasis promoters. *Elife* **3:** e01308.

Naba A, Clauser KR, Whittaker CA, Carr SA, Tanabe KK, Hynes RO. 2014b. Extracellular matrix signatures of human primary metastatic colon cancers and their metastases to liver. *BMC Cancer* **14:** 518.

Oghiso Y, Matsuoka O. 1979. Distribution of colloidal carbon in lymph nodes of mice injected by different routes. *Jpn J Exp Med* **49:** 223–234.

O'Grady P, Thai TC, Saito H. 1998. The Laminin–Nidogen complex is a ligand for a specific splice isoform of the transmembrane protein tyrosine phosphatase LAR. *J Cell Biol* **141:** 1675–1684.

Oskarsson T, Acharyya S, Zhang XHF, Vanharanta S, Tavazoie SF, Morris PG, Downey RJ, Manova-Todorova K, Brogi E, Massague J. 2011. Breast cancer cells produce tenascin C as a metastatic niche component to colonize the lungs. *Nat Med* **17:** 867–874.

Padua D, Zhang XH, Wang Q, Nadal C, Gerald WL, Gomis RR, Massague J. 2008. TGFβ primes breast tumors for lung metastasis seeding through angiopoietin-like 4. *Cell* **133:** 66–77.

Pedrola N, Devis L, Llauradó M, Campoy I, Martinez-Garcia E, Garcia M, Muinelo-Romay L, Alonso-Alconada L, Abal M, Alameda F, et al. 2015. Nidogen 1 and nuclear protein 1: novel targets of ETV5 transcription factor involved in endometrial cancer invasion. *Clin Exp Metastasis* **32:** 467–478.

Peinado H, Lavotshkin S, Lyden D. 2011. The secreted factors responsible for pre-metastatic niche formation: old sayings and new thoughts. *Semin Cancer Biol* **21:** 139–146.

Peinado H, Aleckovic M, Lavotshkin S, Matei I, Costa-Silva B, Moreno-Bueno G, Hergueta-Redondo M, Williams C, Garcia-Santos G, Ghajar CM, et al. 2012. Melanoma exosomes educate bone marrow progenitor cells toward a pro-metastatic phenotype through MET. *Nat Med* **18:** 883–891.

Perbal B. 2006. The CCN3 protein and cancer. In *New trends in cancer for the 21st century* (ed. Llombart-Bosch A, et al.), pp. 23–40. Springer, Netherlands.

Perbal B, Zuntini M, Zambelli D, Serra M, Sciandra M, Cantiani L, Lucarelli E, Picci P, Scotlandi K. 2008. Prognostic value of CCN3 in osteosarcoma. *Clin Cancer Res* **14:** 701–709.

Perbal B, Lazar N, Zambelli D, Lopez-Guerrero JA, Llombart-Bosch A, Scotlandi K, Picci P. 2009. Prognostic relevance of CCN3 in Ewing sarcoma. *Hum Pathol* **40:** 1479–1486.

Pollack VA, Fidler IJ. 1982. Use of young nude mice for selection of subpopulations of cells with increased metastatic potential from nonsyngeneic neoplasms. *J Natl Cancer Inst* **69:** 137–141.

Quail DF, Joyce JA. 2013. Microenvironmental regulation of tumor progression and metastasis. *Nat Med* **19:** 1423–1437.

Rappsilber J, Ishihama Y, Mann M. 2003. Stop and go extraction tips for matrix-assisted laser desorption/ionization, nanoelectrospray, and LC/MS sample pretreatment in proteomics. *Anal Chem* **75:** 663–670.

Ren G, Esposito M, Kang Y. 2015. Bone metastasis and the metastatic niche. *J Mol Med* **93:** 1203–1212.

Reticker-Flynn NE, Malta DF, Winslow MM, Lamar JM, Xu MJ, Underhill GH, Hynes RO, Jacks TE, Bhatia SN. 2012. A combinatorial extracellular matrix platform identifies cell–extracellular matrix interactions that correlate with metastasis. *Nat Commun* **3:** 1122.

Sasaki T, Brakebusch C, Engel J, Timpl R. 1998. Mac-2 binding protein is a cell-adhesive protein of the extracellular matrix which self-assembles into ring-like structures and binds β1 integrins, collagens and fibronectin. *EMBO J* **17:** 1606–1613.

Sevenich L, Werner F, Gajda M, Schurigt U, Sieber C, Muller S, Follo M, Peters C, Reinheckel T. 2011. Transgenic expression of human cathepsin B promotes progression and metastasis of polyoma-middle-T-induced breast cancer in mice. *Oncogene* **30:** 54–64.

Shevchenko A, Wilm M, Vorm O, Mann M. 1996. Mass spectrometric sequencing of proteins silver-stained polyacrylamide gels. *Anal Chem* **68:** 850–858.

St Croix B, Rago C, Velculescu V, Traverso G, Romans KE, Montgomery E, Lal A, Riggins GJ, Lengauer C, Vogelstein B, et al. 2000. Genes expressed in human tumor endothelium. *Science* **289:** 1197–1202.

Subramanian A, Tamayo P, Mootha VK, Mukherjee S, Ebert BL, Gillette MA, Paulovich A, Pomeroy SL, Golub TR, Lander ES, et al. 2005. Gene set enrichment analysis: a knowledge-based approach for interpreting genome-wide expression profiles. *Proc Natl Acad Sci* **102:** 15545–15550.

Supek F, Bošnjak M, Škunca N, Šmuc T. 2011. REVIGO summarizes and visualizes long lists of gene ontology terms. *PLoS ONE* **6:** e21800.

Szklarczyk D, Franceschini A, Wyder S, Forslund K, Heller D, Huerta-Cepas J, Simonovic M, Roth A, Santos A, Tsafou KP, et al. 2015. STRING v10: protein–protein interaction networks, integrated over the tree of life. *Nucleic Acids Res* **43:** D447–D452.

Tang H-Y, Beer LA, Tanyi JL, Zhang R, Liu Q, Speicher DW. 2013. Protein isoform-specific validation defines multiple chloride intracellular channel and tropomyosin isoforms as serological biomarkers of ovarian cancer. *J Proteomics* **89:** 165–178.

Tunggal J, Wartenberg M, Paulsson M, Smyth N. 2003. Expression of the nidogen-binding site of the laminin γ1 chain disturbs basement membrane formation and maintenance in F9 embryoid bodies. *J Cell Sci* **116:** 803–812.

Ueda M, Iguchi T, Komatsu H, Kidogami S, Hu Q, Sato K, Ogawa Y, Nambara SHO, Saito T, Sakimura S, et al. 2015. Clinical significance of expression of nephroblastoma overexpressed (NOV) in patients with colorectal cancer. *Anticancer Res* **35:** 6591–6597.

Ulazzi L, Sabbioni S, Miotto E, Veronese A, Angusti A, Gafà R, Manfredini S, Farinati F, Sasaki T, Lanza G, et al. 2007.

Nidogen 1 and 2 gene promoters are aberrantly methylated in human gastrointestinal cancer. *Mol Cancer* **6:** 17.

Uphoff CC, Drexler HG. 2011. Detecting mycoplasma contamination in cell cultures by polymerase chain reaction. *Methods Mol Biol* **731:** 93–103.

Vallacchi V, Daniotti M, Ratti F, Di Stasi D, Deho P, De Filippo A, Tragni G, Balsari A, Carbone A, Rivoltini L, et al. 2008. CCN3/nephroblastoma overexpressed matricellular protein regulates integrin expression, adhesion, and dissemination in melanoma. *Cancer Res* **68:** 715–723.

van de Vijver MJ, He YD, van't Veer LJ, Dai H, Hart AA, Voskuil DW, Schreiber GJ, Peterse JL, Roberts C, Marton MJ, et al. 2002. A gene-expression signature as a predictor of survival in breast cancer. *N Engl J Med* **347:** 1999–2009.

Vasiljeva O, Papazoglou A, Krüger A, Brodoefel H, Korovin M, Deussing J, Augustin N, Nielsen BS, Almholt K, Bogyo M, et al. 2006. Tumor cell–derived and macrophage-derived cathepsin B promotes progression and lung metastasis of mammary cancer. *Cancer Res* **66:** 5242–5250.

Vogel C, Marcotte EM. 2012. Insights into the regulation of protein abundance from proteomic and transcriptomic analyses. *Nat Rev Genet* **13:** 227–232.

Wagenblast E, Soto M, Gutierrez-Angel S, Hartl CA, Gable AL, Maceli AR, Erard N, Williams AM, Kim SY, Dickopf S, et al. 2015. A model of breast cancer heterogeneity reveals vascular mimicry as a driver of metastasis. *Nature* **520:** 358–362.

Wallin U, Glimelius B, Jirstrom K, Darmanis S, Nong RY, Ponten F, Johansson C, Pahlman L, Birgisson H. 2011. Growth differentiation factor 15: a prognostic marker for recurrence in colorectal cancer. *Br J Cancer* **104:** 1619–1627.

Wang H, Fu W, Im JH, Zhou Z, Santoro SA, Iyer V, DiPersio CM, Yu Q-C, Quaranta V, Al-Mehdi A, et al. 2004. Tumor cell α3β1 integrin and vascular laminin-5 mediate pulmonary arrest and metastasis. *J Cell Biol* **164:** 935–941.

Wang Y, Klijn JG, Zhang Y, Sieuwerts AM, Look MP, Yang F, Talantov D, Timmermans M, Meijer-van Gelder ME, Yu J, et al. 2005. Gene-expression profiles to predict distant metastasis of lymph-node-negative primary breast cancer. *Lancet* **365:** 671–679.

Weilbaecher KN, Guise TA, McCauley LK. 2011. Cancer to bone: a fatal attraction. *Nat Rev Cancer* **11:** 411–425.

Yi XY, Wayner EA, Kim Y, Fish AJ. 1998. Adhesion of cultured human kidney mesangial cells to native entactin: role of integrin receptors. *Cell Adhes Commun* **5:** 237–248.

Zhang Y, Xu B, Liu Y, Yao H, Lu N, Li B, Gao J, Guo S, Han N, Qi J, et al. 2012. The ovarian cancer-derived secretory/releasing proteome: a repertoire of tumor markers. *PROTEOMICS* **12:** 1883–1891.

Zhang T, Zhao C, Luo L, Xiang J, Sun Q, Cheng J, Chen D. 2013. The clinical and prognostic significance of CCN3 expression in patients with cervical cancer. *Adv Clin Exp Med* **22:** 839–845.